International Journal of Nanomedicine

Dovepress
Taylor & Francis Group

Open Access Full Text Article

ORIGINAL RESEARCH

An Injectable Ibuprofen Sustained-Release Composite Hydrogel System Effectively Accelerates Diabetic Wound Healing via Anti-Inflammatory Effects and Angiogenesis

Zhibin Li[1], Haijiang Dong[1], Shenyu Yang[2], Ximei Wang[1], Zhen Li[3]

[1]Department of Plastic and Aesthetic Surgery, The First Affiliated Hospital of Zhengzhou University, Zhengzhou, 450052, People's Republic of China; [2]Medical 3D Printing Center, The First Affiliated Hospital of Zhengzhou University, Zhengzhou, 450052, People's Republic of China; [3]Department of Endovascular Surgery, The First Affiliated Hospital of Zhengzhou University, Zhengzhou, 450052, People's Republic of China

Correspondence: Zhen Li, Department of Endovascular Surgery, The First Affiliated Hospital of Zhengzhou University, Zhengzhou, 450052, People's Republic of China, Email lizhen1029@hotmail.com

Purpose: Excessive inflammation in diabetic wounds, driven by hyperglycemia, prolongs healing, increases the risk of non-healing ulcers, and can lead to severe complications such as amputation or life-threatening infections. Recurrent wound infections and prolonged treatment impose significant economic and psychological burdens, drastically reducing patients' quality of life. Modulating the inflammatory response is a promising strategy to accelerate diabetic wound healing. Ibuprofen (IBU), a widely used anti-inflammatory and analgesic agent, has the potential to promote healing by mitigating excessive inflammation and alleviating wound-associated pain. However, its clinical application is hindered by poor water solubility and a short half-life. Therefore, a controlled and sustained-release system for IBU could enhance its therapeutic efficacy in diabetic wound management.

Materials and Methods: Here, we present an in situ multi-crosslinked composite hydrogel system that integrates oxidized alginate (OSA), methacryloylated gelatin (GelMA), and an ibuprofen/amino-modified β-cyclodextrin inclusion complex (IBU/CD-NH_2) via ion crosslinking, photocrosslinking, and Schiff-base reactions.

Results: The optimized hydrogel formulation was synthesized at 35°C, with a P/A molar ratio of 2 and an methacrylamide(MA) volume fraction of 20%. Physicochemical and biocompatibility analyses demonstrated that the IBU-loaded composite hydrogel exhibits enhanced mechanical strength, favorable biocompatibility, tunable degradation, and injectability. This system effectively addresses IBU's solubility and absorption challenges while conforming to wounds of varying shapes and sizes, enabling controlled and sustained drug release. Cellular and animal studies confirmed that the hydrogel continuously and uniformly releases IBU, exerting anti-inflammatory effects while promoting angiogenesis and fibroblast migration. This leads to enhanced granulation tissue formation, collagen deposition, and epidermal regeneration, significantly accelerating wound closure within 14 days.

Conclusion: By simultaneously suppressing inflammation and stimulating tissue regeneration through controlled IBU release, this hydrogel system offers a highly effective strategy for diabetic wound healing and holds strong potential for clinical application.

Keywords: ibuprofen, diabetic wound healing, sustained-release, injectable composite hydrogel system, inflammation

Introduction

Diabetic wounds are severe chronic complications of diabetes, characterized by prolonged healing due to hyperglycemia. This condition not only imposes a significant financial burden but also drastically reduces patients' quality of life.[1,2] Current treatment options remain limited, aside from hypoglycemic therapies, leaving patients at high risk of amputation.[3,4] Therefore, nonsurgical approaches that directly promote wound healing are crucial for improving patient outcomes. Normal wound-healing progresses through four sequential but overlapping phases: hemostasis, inflammation, proliferation, and remodeling.[5] However, diabetic wounds exhibit a persistent inflammatory response driven by excessive inflammatory infiltration caused by

Received: 6 November 2024
Accepted: 28 March 2025
Published: 11 April 2025

hyperglycemia.[3,4] Accumulating evidence suggests that controlling excessive inflammation—by limiting inflammatory cell infiltration and inflammatory factor secretion—is key to accelerating diabetic wound healing.[6–8]

Nonsteroidal anti-inflammatory drugs (NSAIDs) effectively reduce inflammation and pain by inhibiting cyclooxygenase (COX) and suppressing prostaglandin synthesis.[9] Among them, ibuprofen (IBU) is widely used for its potent anti-inflammatory and analgesic properties.[10,11] However, its therapeutic application in diabetic wound healing remains constrained by its short half-life and hydrophobicity, which necessitate high systemic doses that can cause severe side effects, including gastrointestinal ulcers and kidney injury.[12,13] To enhance IBU's therapeutic potential while minimizing adverse effects, a controlled and sustained drug release system is essential to maintain stable drug concentrations at the wound site and reduce systemic exposure. Although various sustained-release drug delivery systems, such as hydrogels and nanofibers, have been explored for topical applications,[10,13–16] IBU's short half-life and hydrophobicity necessitate further optimization to ensure effective therapeutic outcomes.

Hydrogels, with their three-dimensional porous and hydrophilic network structures, are promising candidates for drug delivery and wound dressing applications.[17] They mimic the extracellular matrix (ECM), absorb excess wound exudates, and maintain a moist healing environment.[18–21] Andrgie et al developed a thermosensitive injectable hydrogel incorporating IBU via simple mixing to mitigate excessive inflammation and promote wound healing.[11] However, direct IBU incorporation often results in uneven drug distribution, reducing bioavailability due to its poor water solubility and hydrophobic nature, highlighting the need for an improved hydrogel delivery system.

β-Cyclodextrin (β-CD) is an effective drug carrier due to its unique structure, featuring a hydrophilic exterior and a hydrophobic internal cavity.[22] It has shown potential in addressing IBU's short half-life and hydrophobicity[23] However, further research is needed to develop a β-CD/IBU complex capable of achieving controlled and sustained drug release, optimizing anti-inflammatory effects, and accelerating diabetic wound healing.

Alginates, natural anionic polysaccharides, are widely utilized in wound dressings and biomaterials due to their excellent biocompatibility, low toxicity, and facile gel formation.[24,25] Additionally, they can be chemically modified to introduce reactive groups that facilitate covalent crosslinking with other polymers, such as peptides and proteins, enhancing cell adhesion and proliferation.[26] However, alginate exhibits unstable mechanical and degradation properties,[27,28] which pose challenges for sustained drug delivery in diabetic wounds of varying sizes and shapes.[29] To address these limitations, an injectable, in situ curing hydrogel system with controlled drug release is required. Photocrosslinkable hydrogels offer a viable solution, enabling both in situ injection and curing.[30–32] Methacryloylated gelatin (GelMA), a photosensitive and biocompatible polymer containing arginine-glycine-aspartic acid (RGD) motifs, promotes cell adhesion and is widely used in tissue engineering.[33,34] To enhance the mechanical properties and biofunctionality of alginate-based hydrogels, oxidized alginate (OSA) is synthesized via partial oxidation. Subsequently, β-cyclodextrin-amino (β-CD-NH_2) and GelMA are crosslinked with OSA through Schiff-base reactions between the aldehyde groups of OSA and the amino groups of GelMA and β-CD-NH_2, improving both mechanical integrity and cell adhesion. This composite hydrogel enables injectable application and in situ photocuring for irregularly shaped wounds. Additionally, prior to Schiff-base crosslinking, β-CD-NH_2 forms an inclusion complex with ibuprofen (IBU) through host–guest interactions, ensuring efficient drug loading. This integration facilitates the controlled and sustained release of IBU from the hydrogel matrix.

Based on these advancements, the objective of this study was to develop an IBU-loaded, controlled-release hydrogel system composed of a multi-network structure by modifying natural biomaterials. This system aims to regulate inflammation and accelerate diabetic wound healing by modulating the wound microenvironment. To achieve this, we engineered an in situ, multi-crosslinked composite hydrogel by incorporating highly oxidized OSA, GelMA with tunable methacrylation degrees, and ibuprofen/β-Cyclodextrin-Animo (IBU/β-CD-NH2) inclusion complexes. Crosslinking was achieved through ionic interactions, photopolymerization, and Schiff-base reactions, yielding a hydrogel with enhanced mechanical strength, favorable biocompatibility, tunable degradation, and injectability. This system effectively delivers IBU in a controlled manner, promoting wound healing by reducing inflammation, enhancing cell proliferation, and stimulating angiogenesis. To fully characterize the hydrogel, we evaluated its porous structure, mechanical properties, biocompatibility, swelling behavior, degradation kinetics, and IBU release profile. Furthermore, its effects on macrophage polarization and angiogenesis were investigated both in vitro and in vivo. The therapeutic efficacy of the IBU-loaded hydrogel system was validated in a streptozotocin-induced diabetic mouse model with full-thickness wounds, demonstrating accelerated wound healing (Figure 1).

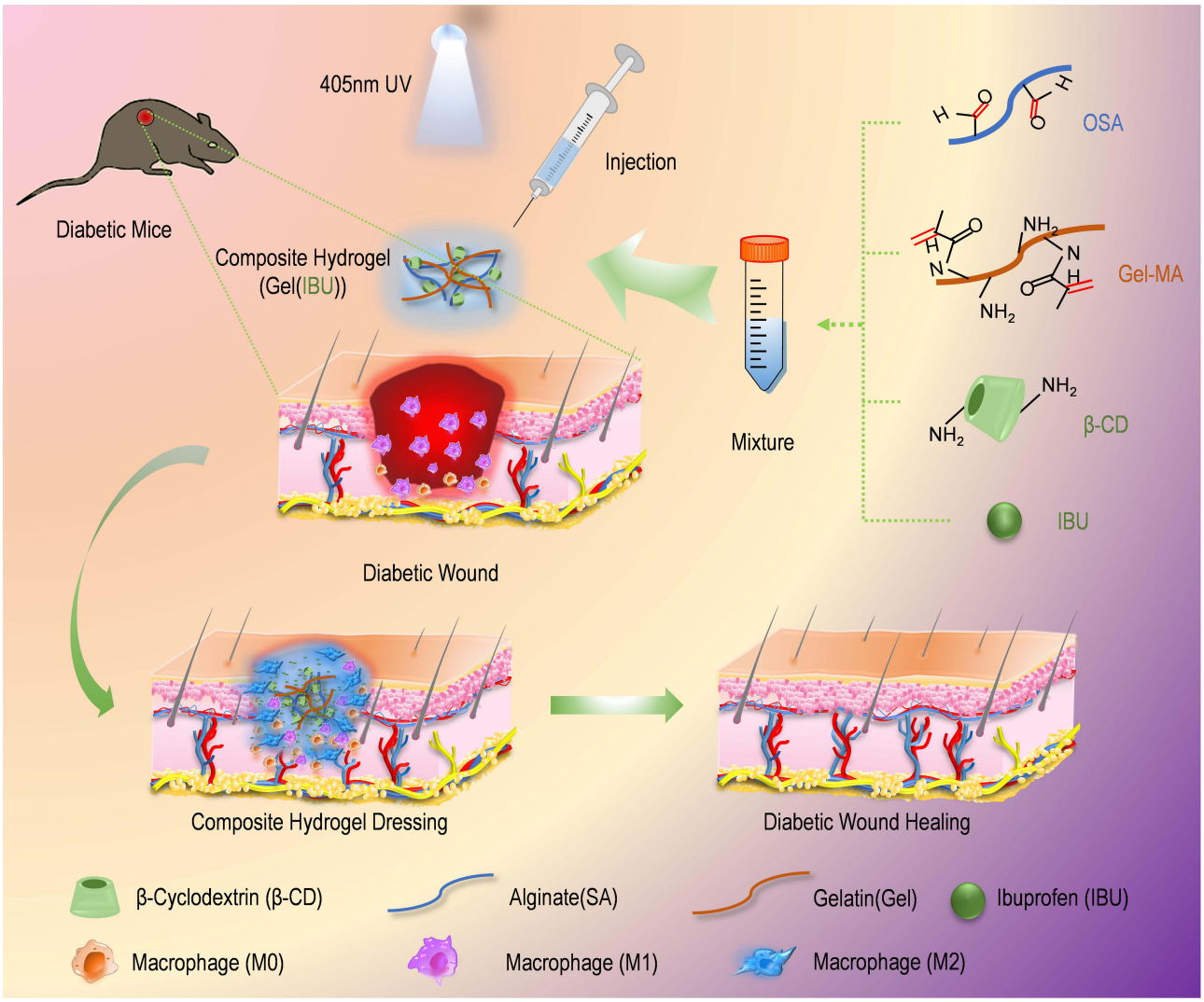

Figure 1 Schematic of the synthesis and application of the IBU-loaded composite hydrogel system.
Abbreviations: OSA, oxidized alginate; GelMA, methacryloylated gelatin; β-CD, β-cyclodextrin.

This composite hydrogel system enables the sustained release of low-dose ibuprofen (IBU), addressing its poor solubility while minimizing the risk of liver, kidney, and cardiac toxicity associated with high-dose oral or systemic administration. Furthermore, it's in situ injection and photocuring capabilities allow precise application to wounds of varying shapes and sizes. The natural materials used in the hydrogel are readily available, easy to process, biocompatible, and cost-effective, offering significant clinical potential. This approach is expected to alleviate both the economic and psychological burdens on patients while enhancing their quality of life.

Materials and Methods

Preparation of Composite Hydrogels

OSA, GelMA, and IBU/CD-NH_2 inclusion complexes were prepared as described in the Supplementary Data (Materials and Methods. OSA (4% w/w) was dissolved in demineralized water under agitation, followed by the addition of GDL (0.75% w/v) to form solution A. Separately, lyophilized GelMA prepolymers were dissolved in PBS (10% w/v) and supplemented with IBU/CD-NH_2 (50 mm), LAP (0.5% w/v), and calcium carbonate (0.3% w/v) to generate solution B. Solutions A and B were mixed at a 1:1 volume ratio and stirred until homogeneous. The resulting solution was injected and UV crosslinked (405 nm) to form a composite hydrogel.

https://doi.org/10.2147/IJN.S504924

Cell Lines and Cell Cultures

Raw 264.7 macrophages, L929 fibroblasts, and MVUEC endothelial cells were obtained from the Cell Bank of the Chinese Academy of Sciences Typical Culture Preservation Committee. Cells were maintained in Dulbecco's Modified Eagle's Medium (Gibco) supplemented with 10% fetal bovine serum (FBS; Clark) and 1% penicillin-streptomycin (P/S; Solarbio, China) under standard culture conditions (37°C, 5% CO_2).

Characterizations of the Hydrogels

Fourier-transform infrared spectroscopy (FTIR) was used to confirm the functional groups of OSA and GelMA using a Spectrum Two FTIR spectrometer (PerkinElmer, Shelton, CT, USA). Spectra were recorded with 30 scans across a frequency range of 4000–500 cm^{-1} at a resolution of 4 cm^{-1}.

Nuclear magnetic resonance (NMR) spectroscopy: The chemical structures of the gel and GelMA were characterized via NMR spectroscopy (Bruker, Germany) at room temperature with a 400 MHz frequency.

Scanning electron microscopy (SEM): The morphology of the composite hydrogels was analyzed using scanning electron microscopy (SEM; LEO153VP, Carl Zeiss, Jena, Germany) at 5.0 kV. Hydrogel samples were freeze-dried, cryofractured, and sputter-coated with a thin gold layer. SEM images were processed using ImageJ software to assess the porous structure.

Transmission electron microscopy (TEM): Transmission electron microscopy (TEM; JEM-1400) was employed to examine the morphology of IBU/CD-NH_2 samples. Aqueous dispersions were deposited onto copper grids with a carbon support film and dried at room temperature. Particle size distribution was analyzed from TEM images using ImageJ software.

Mechanical properties: The mechanical properties of the composite hydrogels were assessed using a universal testing machine. Fully swollen hydrogel samples (1.0 cm × 1.0 cm × 0.8 cm) were subjected to compression at a rate of 5 mm/min under a 10 N tensile load at room temperature. The corresponding stress–strain curves were recorded. Each hydrogel type was tested at least three times, and the average values were reported.

Swelling properties: Lyophilized hydrogel samples were weighed (W_d) and immersed in PBS (pH 7.4) at 37°C. At predefined intervals, the swollen hydrogels were removed, and their surface water was gently blotted before weighing (W_s). The swelling ratio (Qs) was calculated via the following equation: Q_s (%) = $(W_s-W_d)/W_d\times$ 100%.

Self-degradation properties: Hydrogel degradation was quantified by mass loss. Lyophilized samples were initially weighed (W_0), incubated in PBS at 37°C, and retrieved at designated time points for lyophilization and re-weighing (W_1). The remaining mass ratio was calculated via the following equation: Remaining mass percentage = W_1/W_0 × 100%. The percentage degradation was quantified in terms of weight loss via the following equation:

Release of IBU: A 200-μL hydrogel sample was immersed in 2 mL PBS and incubated at 37°C. At predetermined time points (1, 2, 3, 4, 5, 6, and 7 h), 20 μL of supernatant was collected and replaced with an equal volume of fresh PBS. The absorbance at 220 nm was measured using a UV–vis spectrometer, and the ibuprofen (IBU) concentration was determined via a pre-established calibration curve.

Biocompatibility and Cytotoxicity Assay: Hydrogel biocompatibility and cytotoxicity were evaluated using a Cell Counting Kit-8 (CCK-8, Glpbio, USA) and a live/dead cell staining assay (Dojindo, Japan) following the manufacturers' protocols. Cell viability was assessed by incubating cells with hydrogel extracts of varying compositions.

Preparation of Macrophage-Conditioned Media

RAW264.7 macrophages were seeded in a 6-well plate (5×10^5 cells per well) and exposed to Gel, Gel-IBU (25 μg/L), Gel-IBU (50 μg/L), or Gel-IBU (75 μg/L) extracts for 24 h. The culture medium was then collected and centrifuged (1500 rpm, 5 min). The conditioned media from Gel, Gel-IBU (25 μg/L), Gel-IBU (50 μg/L), and Gel-IBU (75 μg/L) were labeled CM-M0, CM-M2 (25 μg/L), CM-M2 (50 μg/L), and CM-M2 (75 μg/L), respectively.

Tube Formation Assay

Matrigel (50 μL) was added to a 96-well plate and allowed to gel at 37°C for 30 min. MUVECs (1×10^5 cells per well) were seeded on the Matrigel and incubated with conditioned media for 12 or 18 h. Tube formation was visualized using optical microscopy, and the number of nodes and tubes was quantified using ImageJ's Angiogenesis Analyzer.

Scratch Assay

L929 cells (1×10^6 per well) were seeded in a 6-well plate and serum-starved in FBS-free medium for 24 h. A standardized linear scratch was introduced, and cells were incubated with conditioned media for 0, 6, 12, or 24 h. The scratched area was observed under an inverted microscope (Leica DM IL LED, Germany), and images were captured with a CCD camera (Leica DFC 420C, Germany). Cell migration was quantified using ImageJ.

Immunofluorescence Staining

Cells and tissue samples were fixed in 4% paraformaldehyde for 10 min at room temperature (RT), followed by three PBS washes. Permeabilization was performed with 0.2% Triton-X 100 for 10 min, and blocking was carried out using 5% bovine serum albumin for 1 h at RT. Samples were then incubated overnight at 4°C with primary antibodies against CD86/iNOS and CD206/ARG1. After thorough washing, they were treated with iFluor™ 488-conjugated goat anti-rabbit IgG and iFluor™ 594-conjugated goat anti-rabbit IgG secondary antibodies at RT for 1 h. Nuclei were counterstained with 4,6-diamidino-2-phenylindole (DAPI) for 15 min at RT. Immunofluorescence signal quantification was performed using ImageJ, measuring positively stained cells in three randomly selected microscopic fields.

Wound-Healing Model in vivo

A type I diabetic C57BL/6 mouse model was established using streptozocin (STZ). Sixty STZ-induced diabetic mice (18–20 g) were randomly assigned to three groups (n = 20 per group): (1) PBS-treated control, (2) OSA-GelMA-CD-NH_2 (Gel)-treated, and (3) OSA-GelMA-IBU/CD-NH_2 (Gel-IBU)-treated. A 1 cm full-thickness circular wound was created on the dorsal skin of each mouse, and a 1 mm thick silicone splinting ring was sutured around the wound. Hydrogels (100 μL) were applied to the wound surface, photopolymerized with visible light (405 nm) for 30s, and covered with 3 M Tegaderm Transparent Dressing. Wound images were captured on days 0, 3, 7, 10, and 14 using a digital camera. Wound-healing rates were analyzed using ImageJ software. The wound-healing rate = $[A_0 - A_{(n)}/A_0] \times 100\%$, where A_0 and $A_{(n)}$ denote the unhealed wound areas on day 0 and day n, respectively.

All animal experiments adhered to the Chinese guidelines for the Ethical Review of Welfare of Laboratory Animals (GB/T 35892-2018) and were approved by the Laboratory Animal Welfare and Ethics Committee of Zhengzhou University (Approval No. 2024-KY-0753-001).

Histology and Immunofluorescence Analysis

Mice were euthanized, and full-thickness skin tissues from the wound periphery were collected on days 3, 7, 10, and 14. Tissue samples were fixed in 4% paraformaldehyde for 24 h, embedded in paraffin, and sectioned into 5 μm thick slices for histological analysis. Hematoxylin-eosin and Masson's trichrome staining were performed to assess wound healing and collagen deposition. Stained sections were imaged using an optical microscope (Olympus, Tokyo, Japan), and collagen deposition was quantified via ImageJ software. Immunofluorescence staining was conducted for CD31 and α-SMA to evaluate neovascularization, while F4/80 (total macrophage marker), iNOS and CD86 (M1 macrophage markers), and ARG1 and CD206 (M2 macrophage markers) were used to assess macrophage polarization and inflammation in wound tissues.

Statistical Analyses

Statistical analyses were conducted using GraphPad Prism 8.0 (GraphPad Software Inc., San Diego, CA). Data are presented as means ± SD and analyzed via one-way ANOVA or *t*-test, with $P<0.05$ considered statistically significant, and n=3-5.

Results

Synthesis and Characterization of OSA, IBU/CD-NH_2 and GelMA

Sodium alginate contains vicinal hydroxyl groups that can be selectively oxidized to aldehyde groups using sodium periodate ($NaIO_4$), forming OSA (Figure 2A). To optimize the oxidation degree (OD), we investigated the effects of reaction temperature and sodium periodate-to-alginate (P/A) molar ratio. The OD of OSA increased with both parameters

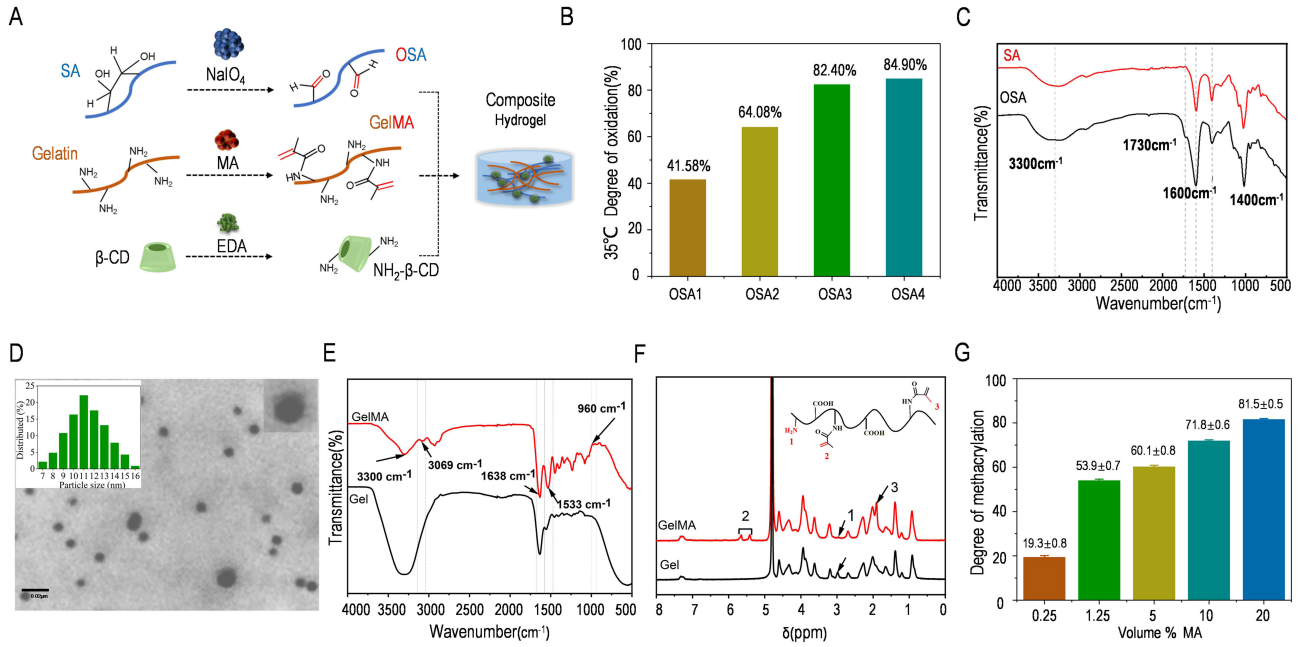

Figure 2 Synthesis, modification, and characterization of each hydrogel. (**A**) Modification method and synthesis diagram of each hydrogel. (**B**) The highest OD of up to 84.9% of OSA was achieved at a reaction temperature of 35°C and a P/A molar ratio of 2. (**C**) FTIR results confirmed the successful preparation of OSA. (**D**) TEM image of the fabricated IBU/CD-NH_2 inclusion complex. Scale bar = 0.02 μm. (**E** and **F**). FTIR (**E**) and ^{1}H NMR (**F**) results confirmed the successful modification of GelMA. (**G**) Results of GelMA with different degrees of methacrylation.

(Figures 2B and S1), reaching a maximum of 84.9% at a reaction temperature of 35°C and a P/A molar ratio of 2, indicating the highest aldehyde content. These optimized conditions were used in subsequent studies. Fourier-transform infrared spectroscopy (FTIR) confirmed aldehyde formation, as evidenced by a new characteristic peak at 1730 cm^{-1}, attributed to the C=O stretching vibration of the aldehyde group (Figure 2C). TEM was used to characterize the morphology, size, and dispersity of the fabricated IBU/CD-NH_2 inclusion complex. The complex exhibited a predominantly spherical shape, with a uniform particle size distribution and an average diameter of 11.5 nm (Figure 2D). This inclusion complex effectively enhances the solubility and hydrophilicity of IBU, overcoming its inherent poor solubility and hydrophobicity. Further characterization of GelMA involved FTIR and proton ^{1}H NMR spectroscopy. Compared to pristine gelatin, GelMA exhibited a shift in the amide II band from 1552 cm^{-1} to 1533 cm^{-1}, confirming successful chemical modification (Figure 2E). ^{1}H NMR spectra further verified the introduction of methacrylamide (MA) groups, with distinct signal shifts: a decreased signal at ~2.9 ppm, corresponding to the methylene protons of lysine, a new peak at 1.8 ppm, indicative of MA methyl groups, and additional peaks at 5.3 ppm and 5.7 ppm, corresponding to methacrylate double-bond protons (Figure 2F). These findings confirm successful MA grafting onto gelatin molecules.

GelMA samples with varying degrees of methacrylation were synthesized by altering MA concentrations. The TNBS assay quantified the degree of substitution (DS), revealing methacrylation degrees of 19.3% ± 0.8%, 53.9% ± 0.7%, 60.1% ± 0.8%, 71.8% ± 0.6%, and 81.5% ± 0.5%, corresponding to MA volume percentages of 0.25%, 1.25%, 5%, 10%, and 20%, respectively (referred to as 0.25%, 1.25%, 5%, 10%, and 20% GelMA) (Figure 2G). Based on these findings, we selected OSA4 (35°C, P/A = 2) and three GelMA formulations (0.25%, 1.25%, and 20%) for subsequent investigations.

Physiochemical Characterization of the Composite Hydrogels

To assess the impact of GelMA with varying degrees of methacrylation on the physicochemical properties of composite hydrogels, three formulations were synthesized by adjusting the methacrylation degree of GelMA (0.25%, 1.25%, and 20%) (Figure 3A). SEM imaging revealed a uniform, well-interconnected pore structure within the hydrogels, where increased methacrylation resulted in much more compacted interior structure (Figure 3B). Pore sizes ranged from

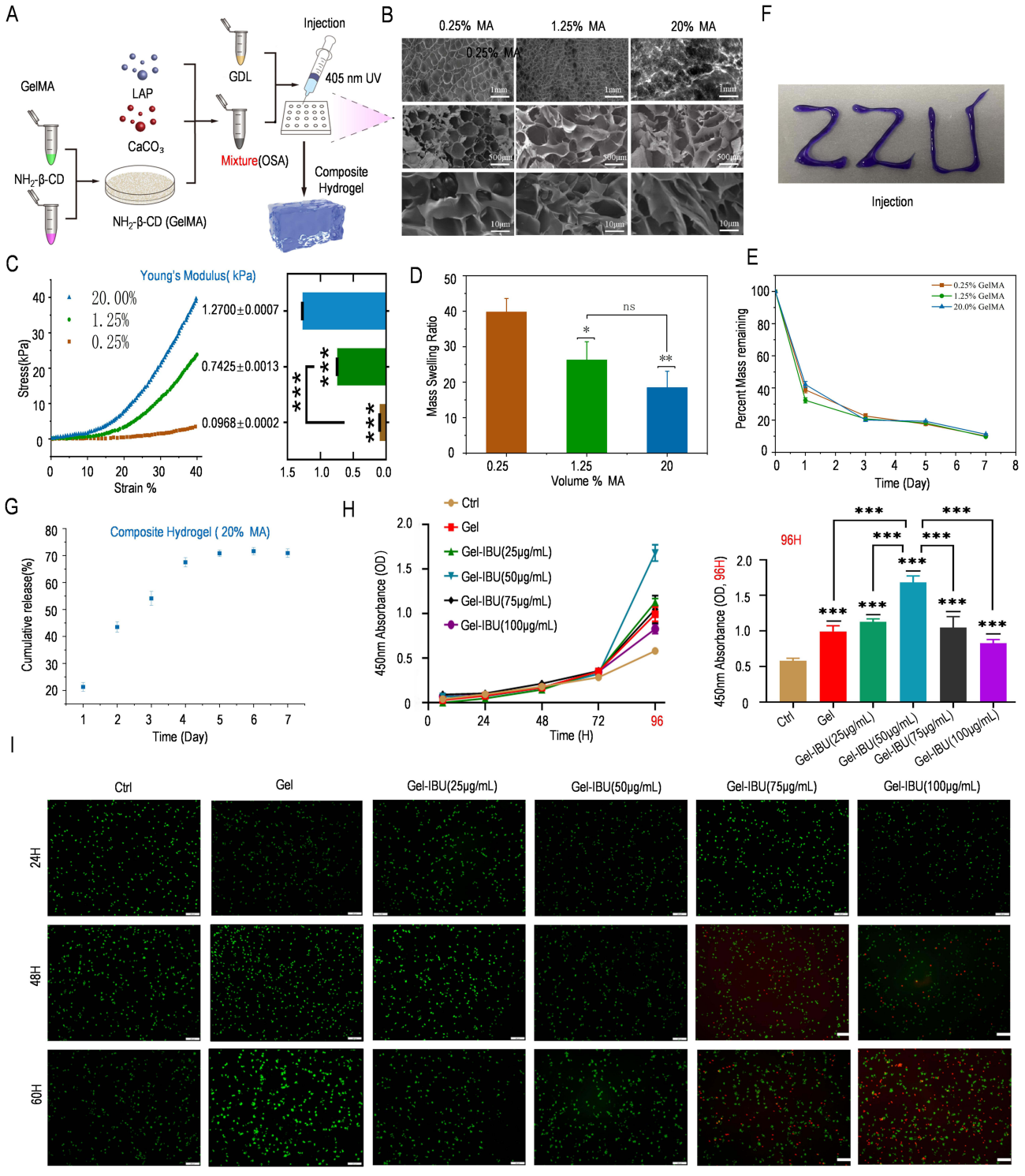

Figure 3 Synthesis and characterization of the composite hydrogel system. (**A**) Synthesis diagram of the composite hydrogel system. (**B**) SEM images revealed the microstructure of the composite hydrogel system. (**C**) Stress–strain curve revealed that the 20% MA mixture in the composite hydrogel system presented the best mechanical properties. (**D**) The 20% MA composite hydrogel system presented the lowest swelling ratio. (**E**) Quantified degradation results of the composite hydrogel system. (**F**) Injection test of the composite hydrogel system. (**G**) Release curve of IBU from the composite hydrogel system. (**H** and **I**) CCK-8 and 96-hour differential analysis of cell proliferation status (**H**), live/dead cell staining (**I**) results revealed the good biocompatibility of the composite hydrogel system. (All the data are shown as the mean ± SD and were analyzed using one-way ANOVA. n=3, *p< 0.05, **p < 0.005, ***p < 0.001, ****p < 0.0001).

Abbreviation: ns, not significant.

https://doi.org/10.2147/IJN.S504924

approximately 50 to 80 μm, with the densest and smallest pores observed in the 20% MA group, attributed to the higher number of photocrosslinking sites. This denser porous network enhances tissue exudate absorption and facilitates nutrient and oxygen exchange. Mechanical analysis via stress–strain curves and Young's Modulus demonstrated that hydrogel stiffness increased with methacrylation, likely due to a higher crosslinking density. The 20% MA group exhibited the most robust mechanical properties (Figures 3C and S2A). For wound-healing applications, optimal swelling properties are crucial—excess exudate absorption maintains a moist environment, promoting healing, while excessive swelling can compress granulation tissue and impede recovery. Swelling ratio analysis revealed an inverse relationship with methacrylation degree (Figures 3D and S2B), attributed to increased porosity in low-methacrylated GelMA. The 20% MA hydrogel exhibited the lowest swelling ratio (1900%), corresponding to its dense network. Hydrogel degradation was quantified by measuring residual mass in PBS over time. The results showed no significant differences in degradation rates among the formulations (Figures 3E and S2C). All hydrogels exhibited rapid initial degradation on day 1, with the lowest degradation in the 20% MA group. Thereafter, degradation proceeded steadily, reaching a common residual mass of 12% by day 7. This stable degradation profile ensures the continuous and controlled release of IBU throughout wound healing. Based on these findings, 20% GelMA was selected for composite hydrogel preparation due to its balanced swelling ratio, degradation profile, and structural stability. The optimized hydrogel was synthesized at 35°C with a P/A molar ratio of 2 and a 20% MA volume fraction. The material could be smoothly injected through an 18G needle, forming a ZZU shape, which is advantageous for treating irregular wound defects (Figure 3F). Rheological test results further demonstrated that within the angular frequency varying from 0.1 to 100 rad/s, the storage modulus (G′) were much greater than the loss modulus (G″) of the composite hydrogels that indicated the mechanical behavior of the hydrogels were stable and suitable for wound dressing once it has been injected (Figure S2D and S2E). This property enables in situ injection and curing, allowing adaptation to various wound shapes and sizes. IBU release from the composite hydrogel exhibited a controlled-release profile. The release curve indicated an initial rapid phase within the first four days, reaching ~70% cumulative release, followed by a sustained, slower release over the subsequent three days. Unlike the rapid hydrogel degradation observed on day 1, IBU release was gradual in the early phase (Figure 3G), possibly due to drug entrapment within the small-molecule network post-molecular fracture. The localized, controlled, and sustained release of low-dose ibuprofen (IBU) mitigates the risk of gastrointestinal and cardiac complications associated with high oral doses. The biocompatibility of the composite hydrogel was assessed using a CCK-8 assay, which confirmed no significant cytotoxicity at IBU concentrations ranging from 0 to 100 μg/mL, indicating good cytocompatibility of Gel-IBU. And the analysis result further showed that Gel-IBU (50 μg/mL) groups exhibiting significantly higher proliferation rates of Raw264.7 cells at 96 hours (Figure 3H). Live/dead cell staining further demonstrated that nearly all Raw264.7 cells remained viable at 24 hours. At 48 and 60 hours, only a few dead cells were observed, primarily in the Gel-IBU (75 μg/mL) and Gel-IBU (100 μg/mL) groups, reinforcing the good biocompatibility of Gel-IBU at 25 and 50 μg/mL (Figure 3I). These findings suggest that IBU promotes macrophage proliferation, particularly at lower concentrations, and that 50 μg/mL is an optimal concentration for subsequent hydrogel preparation.

Gel-IBU Promotes the M2 Phenotype of Macrophages, Tube Formation and Fibroblast Migration in vitro

To evaluate the effects of Gel-IBU composite hydrogels on macrophages, Raw264.7 cells were cultured with LPS and Gel-IBU hydrogel extracts for 48 hours (Figure 4A). Notably, spindle-shaped macrophages, characteristic of M2 polarization, became increasingly prevalent in the Gel-IBU group, while the control group exhibited no morphological changes, retaining their small, round, and pseudopodia-free appearance (Figure 4B). In addition, qPCR results showed that, In addition, qPCR results showed that the expression levels of M2 markers Arg-1 and IL10 in Gel-IBU group were significantly higher than those in Control group, LPS group and Gel group. At the same time, the expression levels of M1 markers iNOS and IL-1β in GEL-IBU group, control group and Gel group were significantly lower than those in LPS group (Figure 4C). Immunofluorescence staining for M1 markers (CD86/iNOS) and M2 markers (CD206/Arg-1) revealed a significantly higher number of CD86/iNOS-positive M1 macrophages in the Gel-IBU group compared to the Gel-only group. Additionally, the Gel-IBU group exhibited the highest number of CD206/Arg-1-positive M2 macrophages,

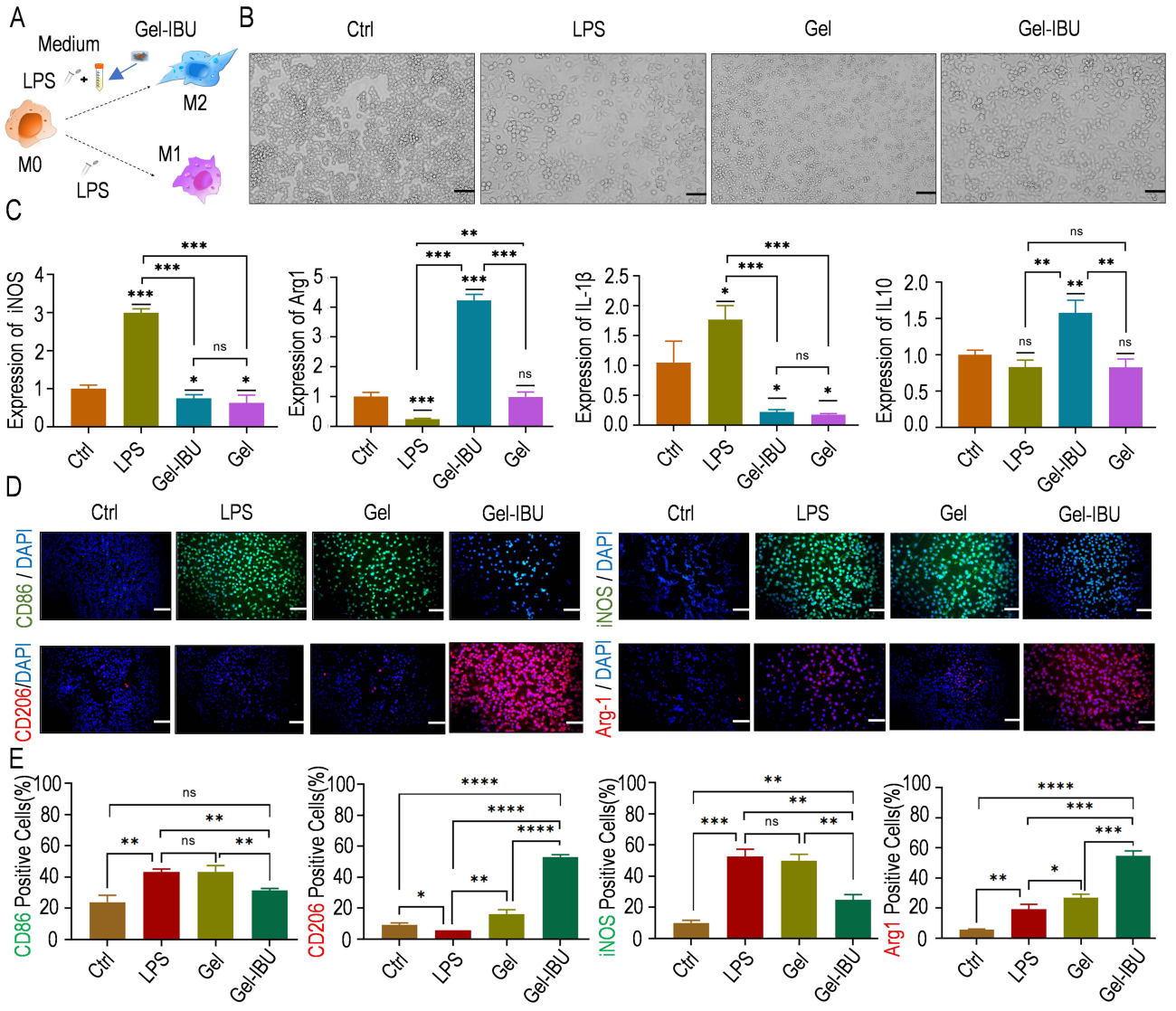

Figure 4 Gel-IBU promotes the M2 phenotype of macrophages. (**A**) Schematic diagram of phenotypic changes in macrophages. Lipopolysaccharide (LPS) (**B**) Morphology of the macrophages changed to the M2 phenotype after Gel-IBU treatment. Scale bar = 50 μm. (**C**) qPCR analysis of M1-related gene (iNOS, IL-1β) and M2-related gene (Arg1, IL-10) expression in macrophages (**D**) Immunofluorescence staining results of the control group and different treatment groups. Scale bar = 100 μm. (**E**) Comparative analysis of the number of cells with positive expression of the corresponding molecular markers in different groups. (All the data are shown as the mean ± SD and were analyzed using one-way ANOVA. n=3, *p< 0.05, **p < 0.005, ***p < 0.001, ****p < 0.0001).
Abbreviation: ns, not significant.

significantly exceeding that of the Gel group (Figures 4D, E, S3 and S4). These findings suggest that Gel-IBU composite hydrogels promote M2 polarization, potentially mitigating inflammation during wound healing. To further investigate the effects of Gel-IBU on endothelial and fibroblast cells, conditioned media (CM) from macrophages pretreated with different IBU concentrations (25, 50, and 75 μg/mL) in Gel-IBU hydrogels were applied to MUVEC and L929 cells. The CCK-8 assay demonstrated that these CM enhanced MUVEC and L929 proliferation, with CM-M2 (25 μg/mL) and CM-M2 (50 μg/mL) groups exhibiting significantly higher proliferation rates at 96 hours (Figure 5A and C). Tube formation assays further confirmed that Gel-IBU-derived M2-CM promoted MUVEC proliferation and angiogenesis. Compared to the control, MUVECs in the CM-M2 group exhibited significantly greater angiogenic capacity, with CM-M2 (25 μg/mL) demonstrating the highest efficiency, forming 29 tubes and 38 nodes (Figure 5B and E). Interestingly, tubule degeneration was more pronounced in the CM-M2 (25 and 50 μg/mL) groups than in others (Figure 5B), indicating that Gel-IBU not only enhances angiogenesis but also delays vascular regression. Furthermore, scratch assays confirmed that Gel-IBU-derived

https://doi.org/10.2147/IJN.S504924

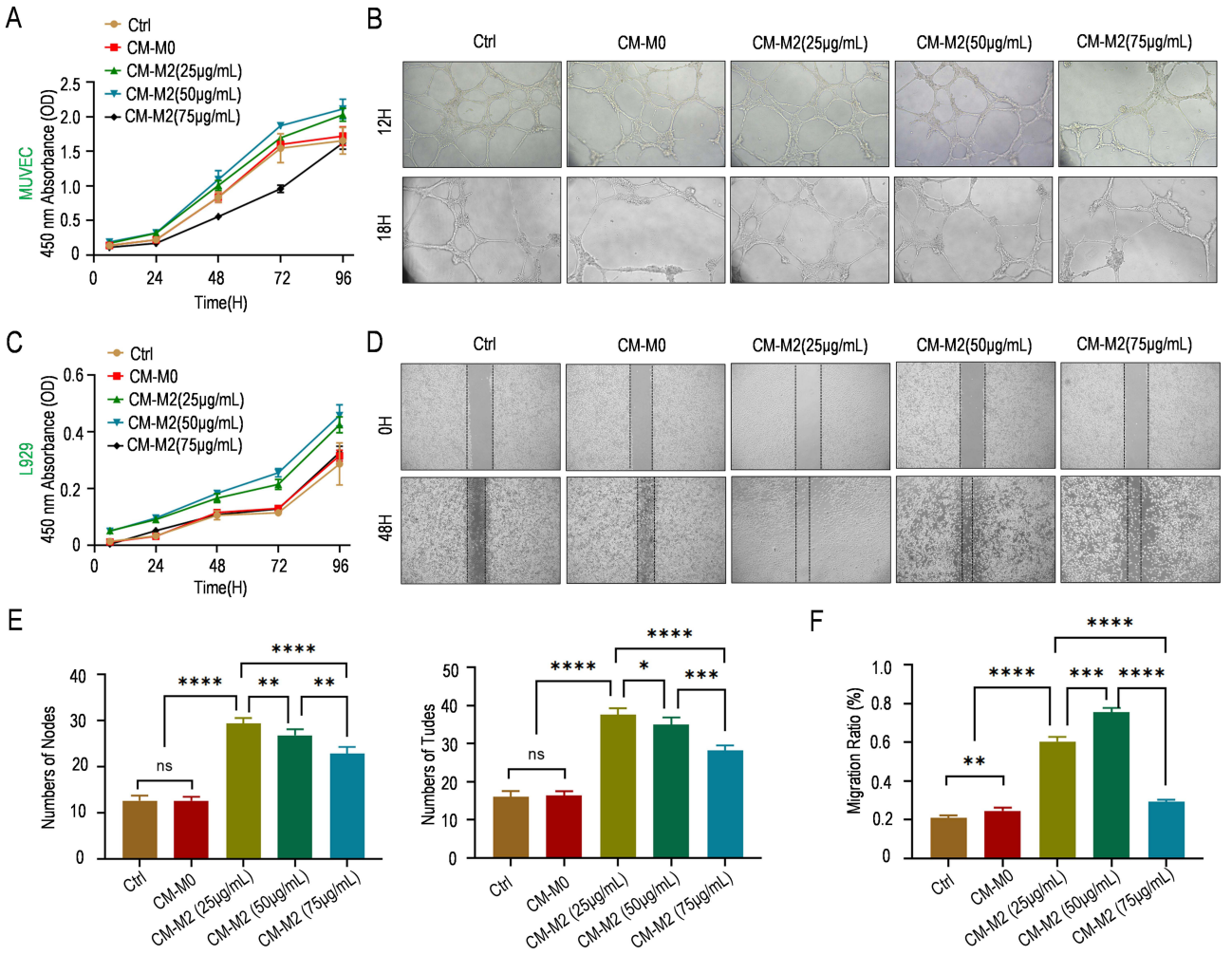

Figure 5 Gel-IBU promotes tube formation and fibroblast migration. (**A**) CCK-8 results for HUVECs treated with different CM. (**B**) Results of the tube formation assay of MUVECs treated with different Gel-IBU-derived M2-CM. Compared to the control, MUVECs in the CM-M2 group exhibited significantly greater angiogenic capacity, with CM-M2 (25 μg/mL) demonstrating the highest efficiency, forming 29 tubes and 38 nodes. (**C**) CCK-8 results for L929 cells treated with different CM. (**D**) Scratch assay results for L929 cells treated with different Gel-IBU-derived M2-CM. (**E**) Statistical results of the number of tube-forming nodes and tubes formed by HUVECs after treatment with different CM. (**F**) Statistical results of the L929 migration ratio after treatment with different CM. (All the data are shown as the mean ± SD and were analyzed using one-way ANOVA. n=3-5, *p< 0.05, **p < 0.005, ***p < 0.001, ****p < 0.0001).
Abbreviation: ns, not significant.

M2-CM significantly promoted L929 cell migration. The CM-M2 (25 μg/mL) and CM-M2 (50 μg/mL) groups exhibited the highest migration ratios after 48 hours, with the CM-M2 (50 μg/mL) group demonstrating the greatest extent of wound closure (Figure 5D and F). These results collectively indicate that Gel-IBU effectively enhances fibroblast migration, contributing to wound healing.

Gel-IBU Accelerates Diabetic Wound Healing in vivo

To evaluate the therapeutic efficacy of the Gel-IBU composite hydrogel, a diabetic wound-healing model was established by injecting the hydrogel into full-thickness excisional wounds in diabetic mice (Figure 6A). Wound-healing progression in three experimental groups—control, Gel, and Gel-IBU—was assessed on days 0, 3, 7, 10, and 14. The results showed no significant difference in wound-healing rates between the control group (33.3%) and the Gel group (33.8%), with both slightly lower than that of the Gel-IBU group (37.4%) on day 3. By day 7, the Gel-IBU group exhibited a significantly higher wound-healing rate (84.4%) compared to the control (53.6%) and Gel groups (59.4%). On day 14, the final wound closure rates were 92.9% (control), 93.3% (Gel), and 98.8% (Gel-IBU), demonstrating the superior healing efficacy of

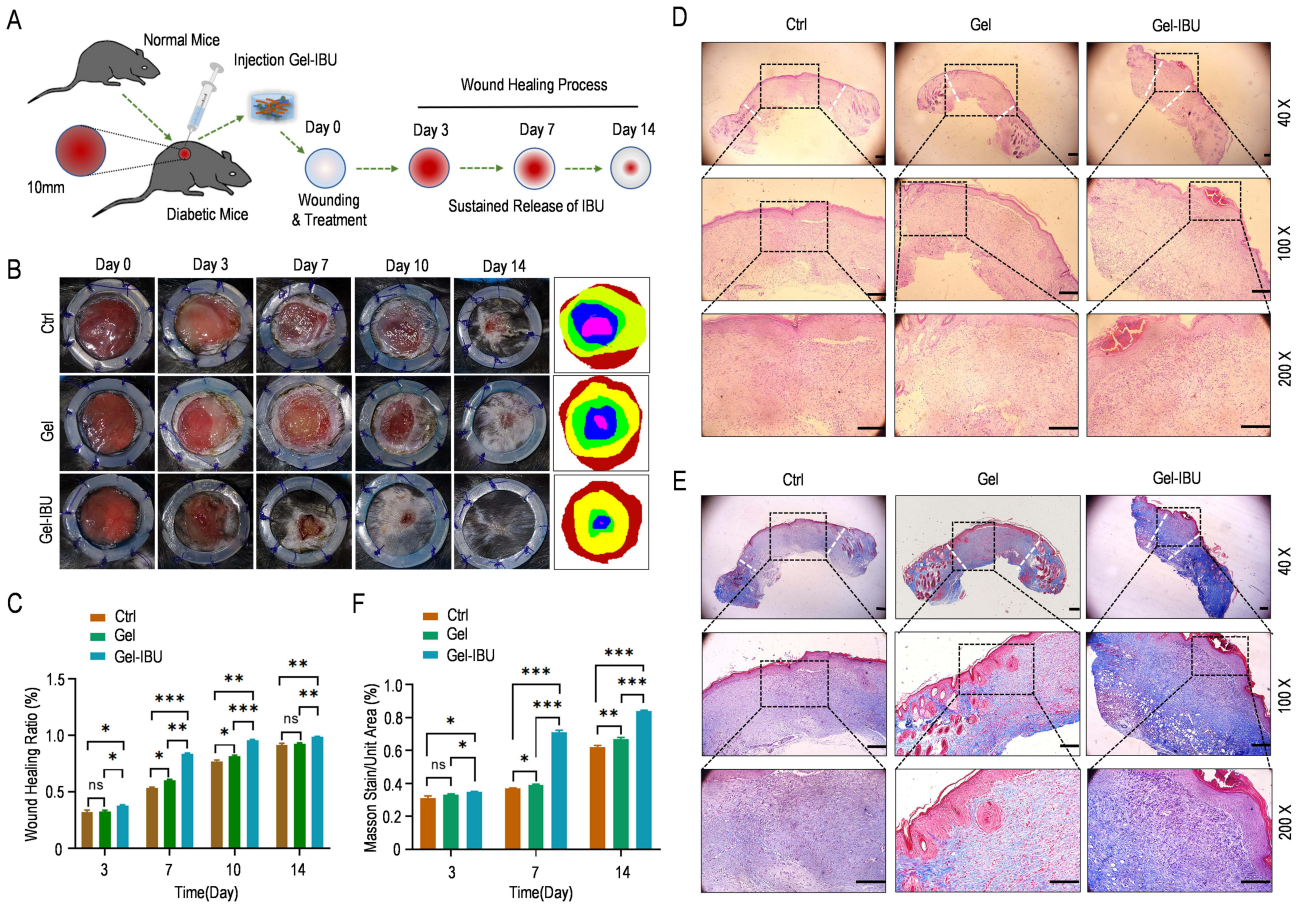

Figure 6 Gel-IBU accelerates diabetic wound healing in vivo. (**A**) Schematic diagram of the establishment of a diabetic wound model and the Gel-IBU treatment process. (**B**) Statistical results of wound-healing assay for the different treatment groups. (**C**) Analysis of the wound-healing ratio in different treatment groups. (**D**) H&E staining results for the different treatment groups. Scale bar = 100 μm. (**E**) Masson's trichrome staining results for the different treatment groups. Scale bar = 100 μm. (**F**) Analysis of Masson's trichrome-stained areas in different treatment groups. (All the data are shown as the mean ± SD and were analyzed using one-way ANOVA. n=3, *p< 0.05, **p < 0.005, ***p < 0.001, ****p < 0.0001).
Abbreviation: ns, not significant.

the Gel-IBU composite hydrogel (Figure 6B and C). Notably, schematic representations of wound sizes at different time points further highlighted the progressive reduction in wound area, indicating that while the Gel hydrogel (without IBU) accelerated diabetic wound healing, its efficacy was lower than that of the Gel-IBU composite (Figure 6B and C).

During the wound proliferation phase, granulation tissue formation is critical for wound filling and re-epithelialization. H&E staining revealed that granulation tissue in the Gel-IBU group was significantly thicker than in the other groups, with newly formed epidermis observed in both the Gel and Gel-IBU groups, whereas it was nearly absent in the control group. These findings aligned with the wound area measurements, showing that Gel-IBU-treated wounds exhibited the highest healing efficiency, with complete re-epithelialization by day 14 (Figures 6D and S5).

Masson's trichrome staining further demonstrated enhanced collagen deposition in the Gel-IBU group, reaching 82.1% on day 14—significantly higher than in the Gel (63.5%) and control (60.5%) groups ($p < 0.001$). Additionally, collagen fibers in the Gel-IBU-treated wounds displayed a more structured and organized arrangement compared to the other groups (Figures 6E, S6 and S7). These results confirm that the Gel-IBU composite hydrogel effectively accelerates diabetic wound healing by promoting granulation tissue formation, epidermal thickening, and collagen organization.

Gel-IBU Can Promote M2 Polarization of Macrophages to Increase Anti-Inflammatory Effects and Promote Angiogenesis Further to Accelerate Diabetic Wound Healing in vivo

To investigate the in vivo effects of Gel-IBU on macrophage polarization, immunofluorescence staining of wound tissues was performed on days 7 and 14 for M1 (CD86/iNOS), M2 (CD206/Arg-1), and pan-macrophage (F4/80) markers.

https://doi.org/10.2147/IJN.S504924

On day 7, the Gel-IBU group exhibited a significant reduction in M1 macrophages (CD86 and iNOS) and an increase in M2 macrophages (CD206 and Arg-1) compared to the control and Gel groups (Figure 7A and B). In contrast, the control and Gel groups showed elevated CD86 and iNOS expression with low CD206 and Arg-1 levels, indicating a sustained inflammatory phase. By day 14, M1 and M2 macrophage populations were notably reduced in the Gel-IBU group, suggesting a diminished inflammatory response and a transition toward wound resolution (Figures 7A, and S8–S19). These findings indicate that Gel-IBU promotes macrophage polarization toward the M2 phenotype, mitigating inflammation and facilitating diabetic wound healing.

CD31 and α-smooth muscle actin (α-SMA) immunofluorescence staining were performed to assess angiogenesis following treatment with different hydrogels for 7 and 14 days. CD31 and α-SMA served as markers for newly formed and mature blood vessels, respectively. On day 7, CD31 expression in the Gel-IBU group was significantly higher than in the other groups, indicating that Gel-IBU enhanced early-stage neovascularization, consistent with the in vitro cell experiments (Figure 7C). By day 14, colocalized CD31 and α-SMA staining was observed in both the Gel and Gel-IBU groups, confirming the formation of mature blood vessels. Notably, the Gel-IBU group exhibited a higher density of CD31 and α-SMA double-positive staining than the Gel group, suggesting that IBU promoted angiogenesis during

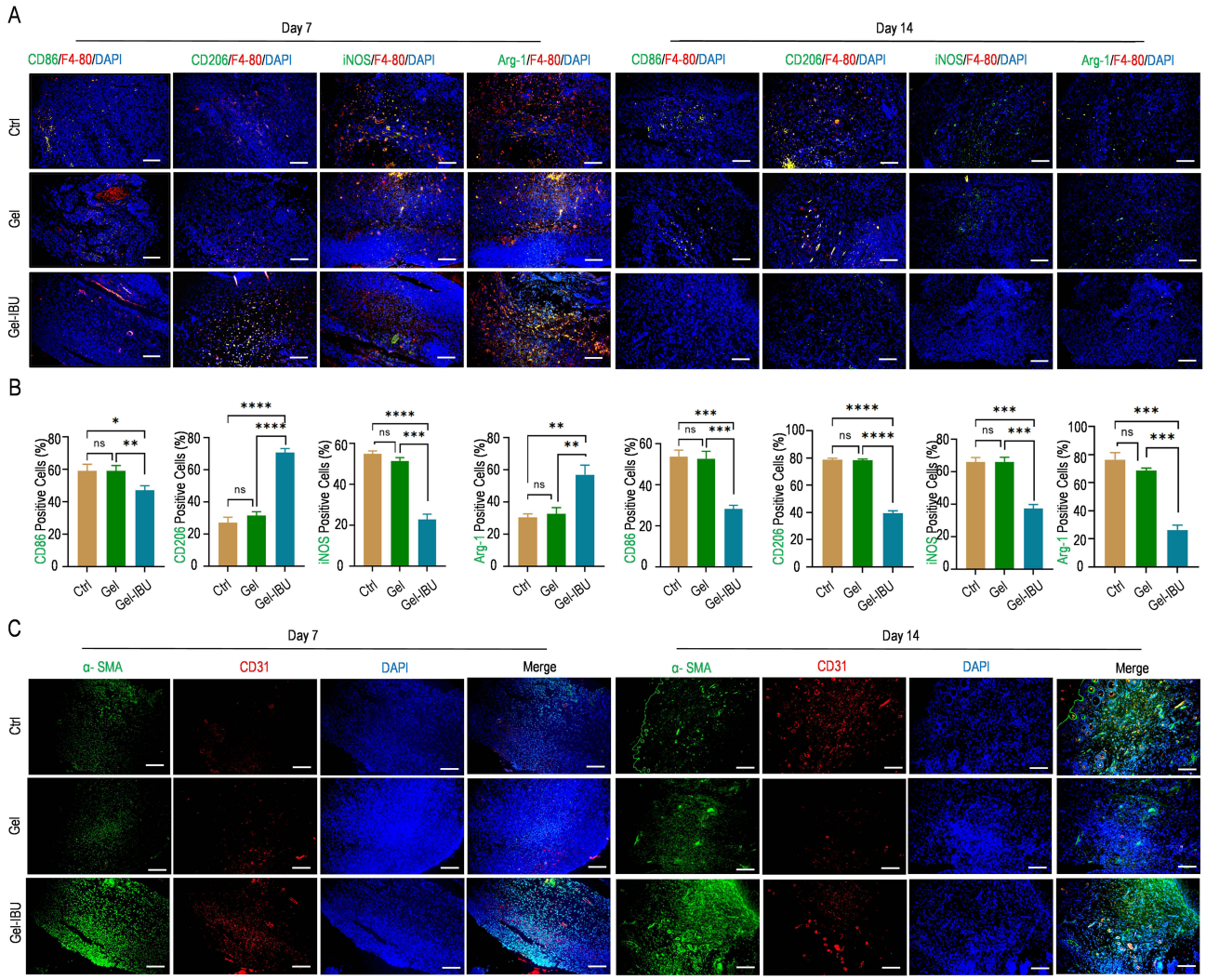

Figure 7 Gel-IBU can promote M2 polarization of macrophages and promote angiogenesis in vivo. (**A**) Immunofluorescence staining results of CD86/iNOS and CD206/Arg-1 expression in different treatment groups on days 7 and 14. Scale bar = 100 μm. (**B**) Statistical analysis of the numbers of CD86/iNOS- and CD206/Arg-1-positive cells in different treatment groups on days 7 and 14. (**C**) Immunofluorescence staining results of CD31 and α-SMA expression in different treatment groups on days 7 and 14. (Scale bar = 100 μm. All the data are shown as the mean ± SD and were analyzed using one-way ANOVA. n=3, *p< 0.05, **p < 0.005, ***p < 0.001, ****p < 0.0001).
Abbreviation: ns, not significant.

diabetic wound healing. These findings indicate that wounds in the Gel-IBU group had either reached the final healing stage or had already healed by day 14. Interestingly, CD31 expression in the control group remained significantly elevated on day 14, suggesting that wound healing in this group was incomplete, with persistent neovascularization indicative of an earlier healing stage. Collectively, these results demonstrate that Gel-IBU effectively promotes angiogenesis and accelerates diabetic wound healing.

Discussion

Diabetic wounds, exacerbated by hyperglycemia-induced excessive inflammation, often result in prolonged healing, non-healing ulcers, and severe complications, including amputation and life-threatening infections. These wounds are increasingly observed in younger patients.[1,4] Conventional treatments, such as blood sugar control and surgical intervention, fail to accelerate wound healing, necessitating repeated treatments that impose financial and emotional strain on patients.[2,35] Controlling the excessive inflammatory response may be key to expediting wound repair. As a nonsteroidal anti-inflammatory drug (NSAID), IBU possesses anti-inflammatory and analgesic properties and may promote diabetic wound healing by mitigating inflammation and reducing pain.[11–13] However, its hydrophobic nature and short half-life[10,23,36] necessitate high systemic doses, increasing the risk of hepatic, renal, gastrointestinal, and cardiovascular complications, thus limiting its clinical utility. A controlled, localized, and sustained drug delivery system could circumvent these limitations. To this end, we designed an injectable IBU-loaded composite hydrogel capable of adapting to wounds of various shapes, offering an effective therapeutic strategy for diabetic wounds.

To enhance IBU solubility and prolong its half-life, we encapsulated it within β-cyclodextrin (β-CD) via host–guest interactions.[37] However, β-CD itself has solubility and bioactivity limitations.[38,39] To overcome these, we synthesized a β-CD derivative, β-cyclodextrin-NH_2 (CD-NH_2),[40] by grafting amino groups (–NH_2) onto β-CD following a modified method from Dou et al. This modification improved the water solubility and biological activity of β-CD, enabling stable IBU encapsulation within its hydrophobic cavities. The hydrogel's primary component, alginate, has inherent drawbacks, including low mechanical strength, unpredictable in vivo degradation, and poor cell adhesion and proliferation support.[27,41,42] To address these issues, we partially oxidized alginate to generate oxidized alginate (OSA), introducing additional reactive groups that facilitate covalent crosslinking with peptides or proteins, enhance cell adhesion and proliferation,[43–45] and enable bonding with β-CD-NH_2 via –NH_2 groups. Additionally, GelMA was crosslinked with OSA through Schiff-base reactions between OSA aldehyde groups and GelMA amino groups, improving the hydrogel's mechanical properties and cell adhesion while maintaining injectability for wound adaptation.[46–48] The photocrosslinking capability further allows in situ curing post-injection, optimizing treatment for irregular wounds.[49] Our findings confirm the composite hydrogel's biocompatibility, injectability, and degradability, with the IBU/CD-NH2 complex uniformly distributed, ensuring sustained and localized drug release. In summary, we successfully developed an affordable, effective, and injectable composite hydrogel system for the controlled release of IBU, adaptable to wounds of diverse shapes and sizes. Photocrosslinked in situ curing is one of the simplest and most effective methods for fabricating wound-healing hydrogels. Moreover, photocrosslink combined with other approaches, such as 3D bioprinting and electrospinning,[50–52] have also been explored for hydrogel preparation, demonstrating promising results in promoting wound healing. Additionally, controlled and sustained drug release can be achieved using nanomaterials or nanoparticles,[53–55] with studies reporting favorable outcomes. Therefore, integrating composite hydrogel systems with nanomaterials or nanoparticles represents a promising direction for future wound treatment research and clinical applications.[56]

Our in vitro cell experiments confirmed that the Gel-IBU composite hydrogel system promotes M2 macrophage polarization and exhibits potential for reducing inflammatory responses during wound healing. These findings were further validated through in vivo animal studies. Angiogenesis, vascular remodeling, and fibroblast migration are critical processes in wound healing.[57,58] Our results indicate that Gel-IBU not only enhances angiogenesis but also regulates vascular remodeling and promotes fibroblast proliferation and migration, as demonstrated by in vitro tube formation and scratch assays. These effects were corroborated by in vivo experimental data, suggesting that the Gel-IBU composite hydrogel effectively facilitates anti-inflammatory responses, angiogenesis, and fibroblast migration. To assess its therapeutic efficacy, we employed a diabetic mouse wound model, wherein Gel-IBU was injected and solidified on the wound surface. By day 14, wounds in the Gel-IBU-treated group had nearly healed, whereas those in the control group remained unhealed. H&E staining revealed significantly thicker granulation tissue and a fully formed, uninterrupted epidermis in the Gel-IBU group, indicating complete wound

closure. Furthermore, Masson's trichrome staining demonstrated markedly greater collagen deposition in the Gel-IBU group compared to controls, with collagen fibers exhibiting a well-organized structure. These results confirm that the Gel-IBU composite hydrogel significantly accelerates diabetic wound healing by promoting granulation tissue formation, enhancing collagen deposition, and facilitating epidermal regeneration.

In summary, we successfully engineered a composite hydrogel system incorporating IBU by modifying natural biomaterials, achieving a cost-effective, convenient, and operable solution. Although various sustained-release drug delivery systems of IBU, such as Polycaprolactone, PLGA, Heparin modified hydrogels and Hyaluronic Acid nanofibers have been explored for wound healing,[13–16] IBU's short half-life and hydrophobicity necessitate have not be solved.[11] This further leads to the need for high doses to achieve therapeutic effects, that can cause severe side effects, including gastrointestinal ulcers and kidney injury. To enhance IBU's therapeutic potential while minimizing adverse effects, a controlled and sustained drug release system is essential to maintain stable drug concentrations at the wound site and reduce systemic exposure. At the same time, for diabetic wounds with different shapes and depths, it is necessary for in-situ injection solidified hydrogel to better adapt to the wound to achieve better therapeutic effects. The sustained and controlled-release hydrogel systems of IBU we developed can solve these problems precisely, and natural hydrogels we used are more biocompatible, biodegradable and non-cytotoxic than synthetic hydrogels. All in all, this system addresses the solubility and absorption challenges of IBU while enabling injectable application for diabetic wounds of varying shapes and sizes. By ensuring the controlled and sustained release of IBU, the hydrogel exerts anti-inflammatory, angiogenic, and fibroblast migration-promoting effects, thereby enhancing granulation tissue formation, collagen deposition, and epidermal regeneration, ultimately accelerating wound healing. Moreover, the system mitigates the risk of gastrointestinal, hepatic, renal, and cardiac complications associated with high-dose oral IBU. IBU primarily exerts its anti-inflammatory effects by inhibiting prostaglandin synthesis, thereby reducing inflammatory mediator release. In addition to its anti-inflammatory properties, IBU also possesses analgesic effects. The Gel-IBU hydrogel system ensures uniform IBU distribution, enabling sustained local analgesia and alleviating patient discomfort. While the current system requires photocuring, in situ curing post-injection may offer a more practical alternative. Recent studies suggest that nanomaterials and microneedles[59] can further optimize drug delivery. Inspired by these advancements, our future research will focus on integrating composite hydrogel systems with nanomaterials or microneedles to establish standardized protocols and develop clinically applicable products.

Conclusion

We present an in situ, multi-crosslinked composite hydrogel system incorporating oxidized sodium alginate (OSA), gelatin methacryloyl (GelMA), and ibuprofen/cyclodextrin-amino (IBU/CD-NH_2) inclusion complexes. The system undergoes ion crosslinking, photocrosslinking, and Schiff-base reactions, enabling controlled gel formation. This IBU-loaded hydrogel is injectable, allowing it to conform to irregular wound surfaces, and it successfully facilitates the sustained and controlled release of IBU. Moreover, it promotes macrophage M2 polarization to mitigate inflammation while enhancing angiogenesis and epidermal regeneration, thereby significantly accelerating diabetic wound healing. This strategy offers an affordable, easily obtainable, and clinically promising solution for diabetic wound treatment.

Acknowledgments

This work was supported by the Henan Provincial Medical Science and Technology Research Joint Venture Project (grant number. LHGJ20240247), Key Research Projects of Higher Education Institutions in Henan Province (grant number. 25A320016) and Science and Technology Assault Project of Henan Province (grant number. 232102311078).

Disclosure

The authors report no conflicts of interest in this work.

References

1. Sun H, Saeedi P, Karuranga S, et al. IDF diabetes atlas: global, regional and country-level diabetes prevalence estimates for 2021 and projections for 2045. *Diabet Res Clin Pract*. 2022;183:109119. doi:10.1016/j.diabres.2021.109119

2. Williams R, Karuranga S, Malanda B, et al. Global and regional estimates and projections of diabetes-related health expenditure: results from the International Diabetes Federation Diabetes Atlas, 9th edition. *Diabet Res Clin Pract*. 2020;162:108072. doi:10.1016/j.diabres.2020.108072
3. Falanga V. Wound healing and its impairment in the diabetic foot. *Lancet*. 2005;366(9498):1736–1743. doi:10.1016/S0140-6736(05)67700-8
4. Burgess JL, Wyant WA, Abdo Abujamra B, Kirsner RS, Jozic I. Diabetic wound-healing science. *Medicina*. 2021;57(10). doi:10.3390/medicina57101072
5. Wang PH, Huang BS, Horng HC, Yeh CC, Chen YJ. Wound healing. *J Chin Med Assoc*. 2018;81(2):94–101. doi:10.1016/j.jcma.2017.11.002
6. Gethin G. Understanding the inflammatory process in wound healing. *Br J Community Nurs*. 2012;17(Suppl):S17–18, S20, S22. doi:10.12968/bjcn.2012.17.sup3.s17
7. Huang C, Dong L, Zhao B, et al. Anti-inflammatory hydrogel dressings and skin wound healing. *Clin Transl Med*. 2022;12(11):e1094. doi:10.1002/ctm2.1094
8. Tian M, Qing C, Niu Y, et al. The relationship between inflammation and impaired wound healing in a diabetic rat burn model. *J Burn Care Res*. 2016;37(2):e115–124. doi:10.1097/BCR.0000000000000171
9. McPherson ML, Cimino NM. Topical NSAID formulations. *Pain Med*. 2013;14(Suppl 1):S35–39. doi:10.1111/pme.12288
10. Liu W, Wang M, Cheng W, et al. Bioactive antiinflammatory antibacterial hemostatic citrate-based dressing with macrophage polarization regulation for accelerating wound healing and hair follicle neogenesis. *Bioact Mater*. 2021;6(3):721–728. doi:10.1016/j.bioactmat.2020.09.008
11. Andrgie AT, Darge HF, Mekonnen TW, et al. Ibuprofen-loaded heparin modified thermosensitive hydrogel for inhibiting excessive inflammation and promoting wound healing. *Polymers*. 2020;12(11):2619. doi:10.3390/polym12112619
12. Morgado PI, Miguel SP, Correia IJ, Aguiar-Ricardo A. Ibuprofen loaded PVA/chitosan membranes: a highly efficient strategy towards an improved skin wound healing. *Carbohydr Polym*. 2017;159:136–145. doi:10.1016/j.carbpol.2016.12.029
13. Johnson KA, Muzzin N, Toufanian S, et al. Drug-impregnated, pressurized gas expanded liquid-processed alginate hydrogel scaffolds for accelerated burn wound healing. *Acta Biomater*. 2020;112:101–111. doi:10.1016/j.actbio.2020.06.006
14. Batool F, Morand DN, Thomas L, et al. Synthesis of a novel electrospun polycaprolactone scaffold functionalized with ibuprofen for periodontal regeneration: an in vitro and in vivo study. *Materials*. 2018;11(4):580. doi:10.3390/ma11040580
15. Chen CT, Chen CH, Sheu C, Chen JP. Ibuprofen-loaded hyaluronic acid nanofibrous membranes for prevention of postoperative tendon adhesion through reduction of inflammation. *Int J mol Sci*. 2019;20(20):5038. doi:10.3390/ijms20205038
16. Riggin CN, Qu F, Kim DH, et al. Electrospun PLGA nanofiber scaffolds release ibuprofen faster and degrade slower after in vivo implantation. *Ann Biomed Eng*. 2017;45(10):2348–2359. doi:10.1007/s10439-017-1876-7
17. Wang Y, Wang Z, Guo W, et al. An injectable extracellular matrix-mimicking conductive hydrogel for sequential treatment of ischemic stroke. *Chem Eng J*. 2024;502:158039. doi:10.1016/j.cej.2024.158039
18. Chen Y, Wang X, Tao S, et al. Research advances in smart responsive-hydrogel dressings with potential clinical diabetic wound healing properties. *Mil Med Res*. 2023;10(1):37. doi:10.1186/s40779-023-00473-9
19. Mi B, Chen L, Xiong Y, et al. Osteoblast/osteoclast and immune cocktail therapy of an exosome/drug delivery multifunctional hydrogel accelerates fracture repair. *ACS Nano*. 2022;16(1):771–782. doi:10.1021/acsnano.1c08284
20. Norouzi M, Nazari B, Miller DW. Injectable hydrogel-based drug delivery systems for local cancer therapy. *Drug Discov Today*. 2016;21(11):1835–1849. doi:10.1016/j.drudis.2016.07.006
21. Gu Z, Huang K, Luo Y, et al. Double network hydrogel for tissue engineering. *Wiley Interdiscip Rev Nanomed Nanobiotechnol*. 2018;10(6):e1520. doi:10.1002/wnan.1520
22. Tian B, Liu Y, Liu J. Smart stimuli-responsive drug delivery systems based on cyclodextrin: a review. *Carbohydr Polym*. 2021;251:116871. doi:10.1016/j.carbpol.2020.116871
23. Nielsen AL, Madsen F, Larsen KL. Cyclodextrin modified hydrogels of PVP/PEG for sustained drug release. *Drug Deliv*. 2009;16(2):92–101. doi:10.1080/10717540802605129
24. Kim NG, Kim SC, Kim TH, et al. Ishophloroglucin A-based multifunctional oxidized alginate/gelatin hydrogel for accelerating wound healing. *Int J Biol Macromol*. 2023;245:125484. doi:10.1016/j.ijbiomac.2023.125484
25. Amiryaghoubi N, Fathi M, Safary A, Javadzadeh Y, Omidi Y. In situ forming alginate/gelatin hydrogel scaffold through Schiff base reaction embedded with curcumin-loaded chitosan microspheres for bone tissue regeneration. *Int J Biol Macromol*. 2024;256(Pt 2):128335. doi:10.1016/j.ijbiomac.2023.128335
26. Oh GW, Kim SC, Kim TH, Jung WK. Characterization of an oxidized alginate-gelatin hydrogel incorporating a COS-salicylic acid conjugate for wound healing. *Carbohydr Polym*. 2021;252:117145. doi:10.1016/j.carbpol.2020.117145
27. Distler T, Kretzschmar L, Schneidereit D, et al. Mechanical properties of cell- and microgel bead-laden oxidized alginate-gelatin hydrogels. *Biomater Sci*. 2021;9(8):3051–3068. doi:10.1039/d0bm02117b
28. Distler T, McDonald K, Heid S, Karakaya E, Detsch R, Boccaccini AR. Ionically and enzymatically dual cross-linked oxidized alginate gelatin hydrogels with tunable stiffness and degradation behavior for tissue engineering. *ACS Biomater Sci Eng*. 2020;6(7):3899–3914. doi:10.1021/acsbiomaterials.0c00677
29. Zhang W, Liu W, Long L, et al. Responsive multifunctional hydrogels emulating the chronic wounds healing cascade for skin repair. *J Control Release*. 2023;354:821–834. doi:10.1016/j.jconrel.2023.01.049
30. Rui K, Tang X, Shen Z, et al. Exosome inspired photo-triggered gelation hydrogel composite on modulating immune pathogenesis for treating rheumatoid arthritis. *J Nanobiotechnology*. 2023;21(1):111. doi:10.1186/s12951-023-01865-8
31. Ling J, Huang T, Wu R, et al. Cell development enhanced bionic silk hydrogel on remodeling immune pathogenesis of spinal cord injury via M2 polarization of microglial. *Adv Funct Mater*. 2023;33(14):2213342. doi:10.1002/adfm.202213342
32. Augustine R, Hasan A, Dalvi YB, et al. Growth factor loaded in situ photocrosslinkable poly(3-hydroxybutyrate-co-3-hydroxyvalerate)/gelatin methacryloyl hybrid patch for diabetic wound healing. *Mater Sci Eng C Mater Biol Appl*. 2021;118:111519. doi:10.1016/j.msec.2020.111519
33. Li S, Sun J, Yang J, et al. Gelatin methacryloyl (GelMA) loaded with concentrated hypoxic pretreated adipose-derived mesenchymal stem cells(ADSCs) conditioned medium promotes wound healing and vascular regeneration in aged skin. *Biomater Res*. 2023;27(1):11. doi:10.1186/s40824-023-00352-3
34. Wang Y, Cao Z, Wei Q, et al. VH298-loaded extracellular vesicles released from gelatin methacryloyl hydrogel facilitate diabetic wound healing by HIF-1α-mediated enhancement of angiogenesis. *Acta Biomater*. 2022;147:342–355. doi:10.1016/j.actbio.2022.05.018

35. Dayya D, O'Neill OJ, Huedo-Medina TB, Habib N, Moore J, Iyer K. Debridement of Diabetic Foot Ulcers. *Adv Wound Care*. 2022;11(12):666–686. doi:10.1089/wound.2021.0016
36. Irvine J, Afrose A, Islam N. Formulation and delivery strategies of ibuprofen: challenges and opportunities. *Drug Dev Ind Pharm*. 2018;44(2):173–183. doi:10.1080/03639045.2017.1391838
37. Pinelli F, Ponti M, Delleani S, et al. β-Cyclodextrin functionalized agarose-based hydrogels for multiple controlled drug delivery of ibuprofen. *Int J Biol Macromol*. 2023;252:126284. doi:10.1016/j.ijbiomac.2023.126284
38. Jiang L, Jiang B, Xu J, Wang T. Preparation of pH-responsive oxidized regenerated cellulose hydrogels compounded with nano-ZnO/chitosan/aminocyclodextrin ibuprofen complex for wound dressing. *Int J Biol Macromol*. 2023;253(Pt 1):126628. doi:10.1016/j.ijbiomac.2023.126628
39. Shin Y, Hu Y, Park S, Jung S. Novel succinoglycan dialdehyde/aminoethylcarbamoyl-β-cyclodextrin hydrogels for pH-responsive delivery of hydrophobic drugs. *Carbohydr Polym*. 2023;305:120568. doi:10.1016/j.carbpol.2023.120568
40. Dou XB, Hu Y, Zhao NN, Xu FJ. Different types of degradable vectors from low-molecular-weight polycation-functionalized poly(aspartic acid) for efficient gene delivery. *Biomaterials*. 2014;35(9):3015–3026. doi:10.1016/j.biomaterials.2013.12.017
41. Rastogi P, Kandasubramanian B. Review of alginate-based hydrogel bioprinting for application in tissue engineering. *Biofabrication*. 2019;11(4):042001. doi:10.1088/1758-5090/ab331e
42. Distler T, Polley C, Shi F, et al. Electrically conductive and 3D-printable oxidized alginate-gelatin polypyrrole: PSS hydrogels for tissue engineering. *Adv Healthc Mater*. 2021;10(9):e2001876. doi:10.1002/adhm.202001876
43. Dananjaya S, Bandara N, Molagoda I, et al. Multifunctional alginate/polydeoxyribonucleotide hydrogels for promoting diabetic wound healing. *Int J Biol Macromol*. 2024;257(Pt 1):128367. doi:10.1016/j.ijbiomac.2023.128367
44. Dalheim MØ, Vanacker J, Najmi MA, Aachmann FL, Strand BL, Christensen BE. Efficient functionalization of alginate biomaterials. *Biomaterials*. 2016;80:146–156. doi:10.1016/j.biomaterials.2015.11.043
45. Volpatti LR, Bochenek MA, Facklam AL, et al. Partially oxidized alginate as a biodegradable carrier for glucose-responsive insulin delivery and islet cell replacement therapy. *Adv Healthc Mater*. 2023;12(2):e2201822. doi:10.1002/adhm.202201822
46. Martyniak K, Kennedy S, Karimzadeh M, et al. Optimizing bioink composition for human chondrocyte expression of lubricin. *Bioengineering*. 2023;10(9):997. doi:10.3390/bioengineering10090997
47. Tang G, Zhu L, Wang W, et al. Alendronate-functionalized double network hydrogel scaffolds for effective osteogenesis. *Front Chem*. 2022;10:977419. doi:10.3389/fchem.2022.977419
48. Seymour AJ, Kilian D, Navarro RS, Hull SM, Heilshorn SC. 3D printing microporous scaffolds from modular bioinks containing sacrificial, cell-encapsulating microgels. *Biomater Sci*. 2023;11(23):7598–7615. doi:10.1039/d3bm00721a
49. Zahid AA, Augustine R, Dalvi YB, et al. Development of nitric oxide releasing visible light crosslinked gelatin methacrylate hydrogel for rapid closure of diabetic wounds. *Biomed Pharmacother*. 2021;140:111747. doi:10.1016/j.biopha.2021.111747
50. Li J, Zhang S, He C, Ling J. Electrospun fibers based anisotropic silk fibroin film with photodynamic antibacterial therapy for S. aureus infected wound healing. *Int J Biol Macromol*. 2024;254(Pt 1):127685. doi:10.1016/j.ijbiomac.2023.127685
51. Ghosal K, Manakhov A, Zajíčková L, Thomas S. Structural and surface compatibility study of modified electrospun Poly(ε-caprolactone) (PCL) composites for skin tissue engineering. *AAPS Pharm Sci Tech*. 2017;18(1):72–81. doi:10.1208/s12249-016-0500-8
52. Khunová V, Kováčová M, Olejniková P, et al. Antibacterial electrospun polycaprolactone nanofibers reinforced by halloysite nanotubes for tissue engineering. *Polymers*. 2022;14(4):746. doi:10.3390/polym14040746
53. Augustine R, Zahid AA, Hasan A, Dalvi YB, Jacob J. Cerium oxide nanoparticle-loaded gelatin methacryloyl hydrogel wound-healing patch with free radical scavenging activity. *ACS Biomater Sci Eng*. 2021;7(1):279–290. doi:10.1021/acsbiomaterials.0c01138
54. Abdolahinia ED, Amiryaghoubi N, Fathi M, Barar J, Omidi Y. Recent advances in injectable nanocomposite hydrogels. *Nano-Struct Nano-Objects*. 2024;39:101254. doi:10.1016/j.nanoso.2024.101254
55. Hamed SH, Azooz EA, Al-Mulla EAJ. Nanoparticles-assisted wound healing: a review. *Nano Biomed Eng*. 2023;15(4):425–435. doi:10.26599/NBE.2023.9290039
56. Augustine R, Prasad P, Khalaf IMN. Therapeutic angiogenesis: from conventional approaches to recent nanotechnology-based interventions. *Mater Sci Eng C*. 2019;97:994–1008. doi:10.1016/j.msec.2019.01.006
57. Peña OA, Martin P. Cellular and molecular mechanisms of skin wound healing. *Nat Rev mol Cell Biol*. 2024;25(8):599–616. doi:10.1038/s41580-024-00715-1
58. Huang X, Liang P, Jiang B, et al. Hyperbaric oxygen potentiates diabetic wound healing by promoting fibroblast cell proliferation and endothelial cell angiogenesis. *Life Sci*. 2020;259:118246. doi:10.1016/j.lfs.2020.118246
59. Yi Y, Yang Z, Zhou C, Yang Y, Wu Y, Zhang Q. Quercetin-encapsulated GelMa hydrogel microneedle reduces oxidative stress and facilitates wound healing. *Nano TransMed*. 2024;3:100030. doi:10.1016/j.ntm.2024.100030